Three-dimensional CaP/gelatin lattice scaffolds with integrated osteoinductive surface

topographies for bone tissue engineering

Biofabrication

PAPER

Three-dimensional CaP/gelatin lattice scaffolds with integrated osteoinductive surface topographies for bone tissue engineering

Danish Nadeem[1], Carol-Anne Smith[2], Matthew J Dalby[2], R M Dominic Meek[3], Sien Lin[4], Gang Li[4,5,6] and Bo Su[1]

1 School of Oral and Dental Sciences, University of Bristol, Bristol BS1 2LY, UK
2 Centre for Cell Engineering, University of Glasgow, Glasgow, G12 8QQ, UK
3 Department of Orthopaedics, Southern General Hospital, Glasgow G51 4TF, UK
4 Department of Orthopaedics and Traumatology, Li Ka Shing Institute of Health Sciences, Faculty of Medicine, The Chinese University of Hong Kong, Prince of Wales Hospital, Shatin, Hong Kong SAR, People's Republic of China
5 Key Laboratory for Regenerative Medicine, Ministry of Education, School of Biomedical Sciences, Faculty of Medicine, The Chinese University of Hong Kong, Hong Kong SAR, People's Republic of China
6 The CUHK-ACC Space Medicine Centre on Health Maintenance of Musculoskeletal System, The Chinese University of Hong Kong Shenzhen Research Institute, Shenzhen, People's Republic of China.

E-mail: b.su@bristol.ac.uk

Keywords: fabrication, scaffolds, microtopography, bone

Abstract

Surface topography is known to influence stem cells and has been widely used as physical stimuli to modulate cellular behaviour including adhesion, proliferation and differentiation on 2D surfaces. Integration of well-defined surface topography into three-dimensional (3D) scaffolds for tissue engineering would be useful to direct the cell fate for intended applications. Technical challenges are remaining as how to fabricate such 3D scaffolds with controlled surface topography from a range of biodegradable and biocompatible materials. In this paper, a novel fabrication process using computer numerically controlled machining and lamination is reported to make 3D calcium phosphate/gelatin composite scaffolds with integrated surface micropatterns that are introduced by embossing prior to machining. Geometric analysis shows that this method is versatile and can be used to make a wide range of lattices with porosities that meet the basic requirements for bone tissue engineering. Both *in vitro* and *in vivo* studies show that micropatterned composite scaffolds with surfaces comprising 40 μm pits and 50 μm grooves were optimal for improved osteogenesis. The results have demonstrated the potential of a novel fabrication process for producing cell-instructive scaffolds with designed surface topographies to induce specific tissue regeneration.

1. Introduction

Bone scaffolding is one of the key elements in tissue engineering, especially for large bone defect regeneration. The principle function of a bone scaffold is to provide support for migration and recruitment of osteoprogenitor cells followed by their proliferation, differentiation and ultimately matrix formation accompanied by remodelling of the bone. An ideal bone scaffold should therefore fulfil several basic requirements, including biocompatibility, mechanical properties, biodegradability, pore size and interconnectivity [1]. A wide range of materials which partially meet above requirements have been used. They range from bioceramics to bioresorbable polymers and a combination of the two (ceramic/polymer composites). Due to the inherently brittle nature of pure ceramics, composite systems are essential in combining the properties of both ceramic and polymeric components to provide potentially desirable mechanical properties. With respect to the development of ceramic/polymer composites, the vast majority of synthetic bone scaffolds are based upon synthetic polymers such as polylactic acid. These have a tendency to undergo rapid hydrolytic degradation *in vivo*, resulting in a rapid loss of mechanical properties and structural integrity and causing a localized inflammatory response due to acidic products [2, 3]. Additionally, many currently available synthetic bone scaffolding solutions raise concerns of toxicity due to

the use of harsh organic solvents, catalysts and in some cases, the formation of cytotoxic degradation products. As such, the use of a biocompatible, containing little or no toxic elements, such as water-soluble gelatin system would be more appropriate [4–6].

One of the most important aspects for successful bone regeneration is the control of cellular response of cells seeded onto a bone scaffold. Generally speaking, there are two ways of induction of a desirable cellular response—either chemical or physical, both of which can be integrated into the design of an effective bone scaffold [7]. Chemical cues for a cellular response can be provided by two main sources. Primarily, an effective materials system, used to make the scaffold, can be selected to induce the required cellular response through employment of bioactive materials with osteoconductive and osteoinductive properties. For example, bioceramic components comprised of calcium phosphate (CaP) ceramics or bioactive glasses can offer substantial benefits, providing both a biocompatible and bioactive environment for cells to be seeded into. Further chemical stimuli can be provided by modification of the biomaterial surface, through the adhesion or incorporation of adsorbable osteogenic or angiogenic factors and proteins, e.g. bone morphogenic proteins (BMP-2), insulin-like and vascular-endothelial growth factors, which can be used to induce and modulate the required cellular response [8].

An alternative to the chemically mediated stimulation of osteogenesis is the presentation of topographical cues that can be used to encourage significant increases in levels of cellular adhesion, proliferation and osteogenic differentiation. Early studies by Swart *et al* demonstrated how changes in topography due to treatment of titanium surfaces resulted in varying degrees of osteoblastic adhesion [9]. Bowers *et al* expanded upon the enhancement of an osteoblastic response through optimization of surface roughness, showing the positive effects that increasing surface roughness can have upon cellular adhesion [10]. Boyan *et al* observed the dependence of osteoblast phenotypic expression in monolayer culture on surface microtopography [11]. Moving on from early studies of roughened surfaces, recent works are more focused on well-defined micropatterns to better elucidate the role of microtopography in cellular mechanotransduction [12]. Micro-pits [13] and micro-grooves [14] are reported to trigger *in vitro* bone formation and be osteoinductive in polymers and ceramics. For bone tissue engineering applications, the challenge is how to integrate such osteoinductive microtopographies into complex three-dimensional (3D) scaffolds.

Bone tissue engineering scaffolds can be generally divided into random foams and regular lattices. The fabrication of random foams includes replication, sacrificial templates and direct foaming methods [15]. Th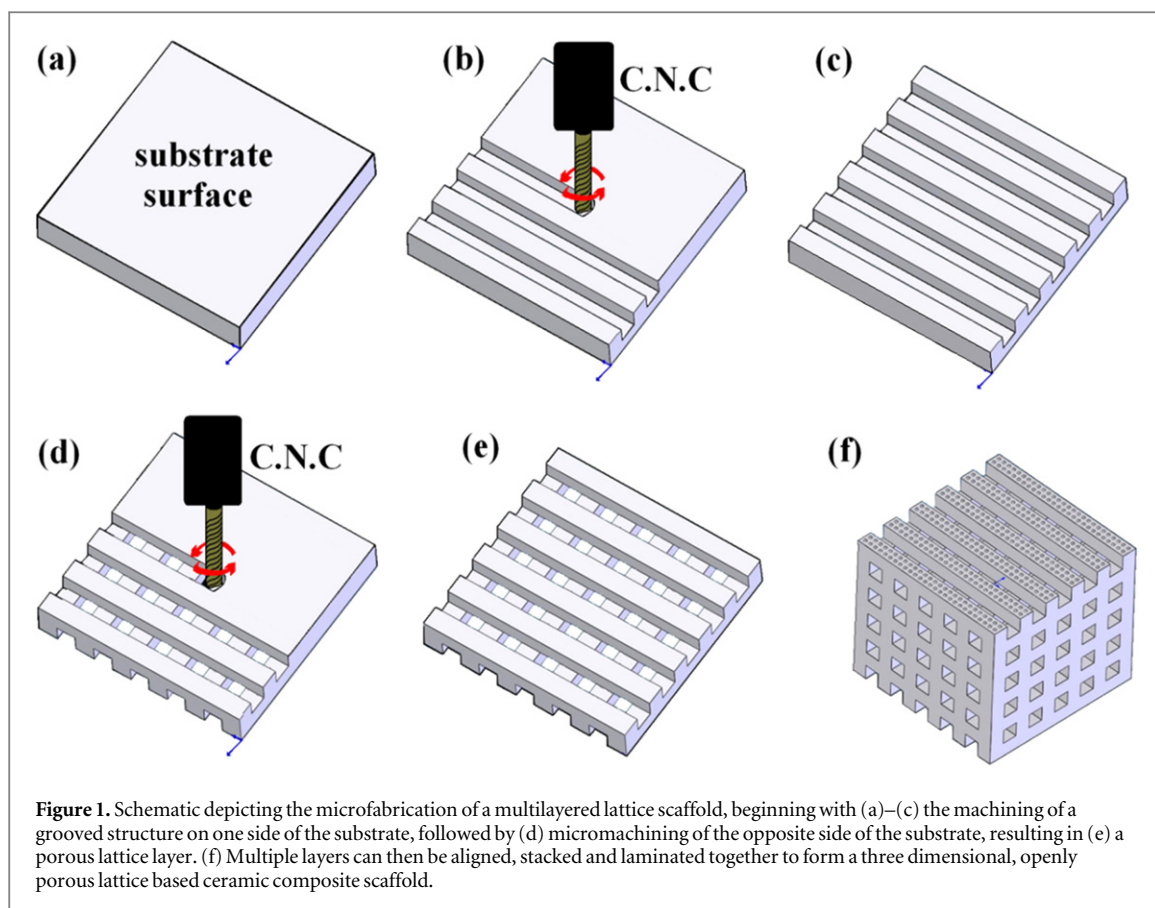e construction of 3D lattice scaffolds is largely realised through 3D printing or solid freeform fabrication (SFF) [16]. SFF is a general approach in which 3D constructs are built up layer-by-layer based on a computer-aided-design file. There are many commercial SFF techniques available for different materials. They include stereolithography, selective laser sintering, 3D printing, fused deposition modelling and microrobotic deposition [17]. Compared to foams, SFF techniques have advantages of enhanced resolution, precise architectural control and customisability; nevertheless it is not trivial to produce 3D bone scaffolds with defined micro-topography. Mata *et al* reported a fabrication technique based on microfabrication and soft lithography to produce 3D scaffolds with precise micro-architecture and surface microtextures [18]. However, the material used was polydimethylsiloxane which is not an ideal material for bone tissue engineering. Cha *et al* demonstrated the fabrication a 3D scaffold with micropatterns using a nanostereolithography technique [19]. The methodology was, however, limited to Ormocer, an organically modified ceramic material which is photocurable but non-degradable. We have developed a subtractive technique to produce an interconnected ceramic structure where ceramic green tapes were computer numerically controlled (CNC) machined and laminated to form 3D lattices [20]. We can use a similar process to fabricate ceramic/polymer composite lattice scaffolds for bone tissue engineering. Most importantly, it is possible to incorporate surface micropatterning into the fabrication process and the process is highly facile. Because pure ceramic scaffolds are brittle, we will focus on ceramic/polymer composite scaffolds in this work to take the advantage of non-brittle mechanical properties of the composite scaffolds.

The objective of this work is to develop, fabricate and evaluate novel 3D CaP/gelatin composite scaffolds for application within the field of bone tissue engineering, because CaP is an osteoconductive material widely used in orthopaedic applications, CaP/gelatin composite can potentially possess better mechanical properties than brittle CaP ceramic. An osteoconductive composite lattice scaffold made of CaP/gelatin will be designed and fabricated using a subtractive microfabrication method with controlled surface microtopography in order to create physical cues for osteoinductivity. Both *in vitro* and *in vivo* characterization will be carried out using human osteoprogenitor cells (hOPCs) and a rabbit model.

2. Experimental

2.1. Raw materials

β-tricalcium phosphate (β-TCP) powder (P304S, D50 $\sim$ 1 μm, Plasma Biotal UK), hydroxylapatite (HA) powder (P260S BM, D50 $\sim$ 3 μm, Plasma Biotal UK) and Type-A gelatin of porcine origin (G2500,

Figure 1. Schematic depicting the microfabrication of a multilayered lattice scaffold, beginning with (a)–(c) the machining of a grooved structure on one side of the substrate, followed by (d) micromachining of the opposite side of the substrate, resulting in (e) a porous lattice layer. (f) Multiple layers can then be aligned, stacked and laminated together to form a three dimensional, openly porous lattice based ceramic composite scaffold.

~300 bloom, Sigma Aldrich, USA), were used in the development and fabrication of ceramic composite substrates and scaffolds. The hydroxyapitite and β-TCP powders were used as received. They are well characterized materials which have been used widely in bone tissue engineering [21].

2.2. Preparation of composite tapes

Ceramic/polymer composite slurry, consisting of HA and β-TCP was prepared with a total ceramic solid content of 40 vol%. The solid loading ratio of HA and β-TCP was set at 60% and 40% respectively, as fractions of the total solid content. Duramax D-3005 (MW $\approx$ 4000 Da, ROHM and HAAS, Germany) was added as a dispersant at 1 wt% by total mass of the ceramic solid content. The polymer phase, consisting of Type-A gelatin at a concentration of 5 wt% by mass of the total water content was injected into the ceramic slurry and stirred for a total of 10 min in a water bath at 40 °C. 0.4% octanol was used as a defoaming agent. The resulting composite slurry was then poured into the reservoir of the doctor blade apparatus and ~120 × 250 mm^2 sections of the composite slurry were tape cast at a height of ~2 mm and a rate of approximately 0.1 mm s^{-1} onto hydrophobically treated acetate sheets. The tape cast substrate was allowed to set at room temperature and was then dried between weighted porous sheets for up to three days.

2.3. Micropatterning of composite tapes

Embossing of substrates was carried out using a universal Testing Machine to compress a substrate between a preformed Ni mask of dimensions 50 × 50 mm^2 and a stainless steel block (50 × 50 mm^2). The Ni masks were fabricated using a standard photolithography and electroplating method [14]. The compressive load applied was increased at a rate of 0.05 MPa s^{-1} up to the required embossing pressure. Transcribed micropatterns (negative images of the mask used) include 50 μm grooves spaced at a distance of 100 μm and 40 μm pits with a pitch distance of 100 μm.

2.4. Lattice fabrication via micromachining and lamination [20]

Fabrication of lattices was carried out using CNC machining (ROLAND Modela MDX-650) of either side of the ceramic composite substrates at room temperature (figure 1), using a vacuum table to fix the machined substrate in place. Fabrication of multiple lattice geometries was carried out using an assortment of 2–4 flute drill bits (size range from 0.3 to 1.0 mm). Inter-lattice lamination was achieved via application of a 5% gelatin solution, by a thin paintbrush, to the unpatterned surface of fabricated lattice layers. Subsequent compression between two glass slides for up to an hour was followed by dehydrothermal crosslinking. Additional crosslinking of the multilayered lattice scaffold was achieved through dipping in a

10 mM genipin (MW = 226.23, Genipin, Challenge Bioproducts Taiwan) solution for 48 h. Genipin (a substance extracted from geniposide) is an intramolecular bridge-linker that has been used in preference to other crosslinking agents such as glutaraldehyde due to its comparatively low level of cytotoxicity [22]. Additionally, genipin also exhibits a good level of biodegradability at low concentrations and allows for a high degree of crosslinking, therefore is widely used as a crosslinking agent for gelatin [23–25]. The combination of dry crosslinking (i.e. dehydrothermal treatment under vacuum) and wet crosslinking (i.e. genipin solution immersion) was designed to preserve the surface micropatterns after scaffold fabrication. The degradation behaviour of optimized composite scaffolds was reported in our previous publication [26].

2.5. Characterization and evaluation of micropatterned composite scaffold

Characterization of embossed micropatterns and machinability was conducted using contact profilometry (Surftest SV-2000, Mitutoyo, Japan), light (HIROX KH-7700 Digital Microscope and digital light transmission microscope LEICA DMLB Digital Microscope) and scanning electron microscopy (JEOL JSM 5600LV).

2.6. *In vitro* evaluation

Cell cultures using hOPCs were conducted in triplicate on composite surfaces with various microtopographies. HOPCs ($P = 2$–3) selected from whole bone marrow by ficol gradient and adherence to tissue culture plastic were seeded onto planar control and micropatterned composite substrate surfaces, at a density of 1×10^4 cells ml^{-1}. All cells were cultured in Dulbecco's modified Eagle's medium (DMEM) (DMEM, PAA Laboratories), supplemented with 10% (v/v) foetal calf serum, sodium pyruvate, 100 × non-essential amino acids and approximately 0.02% (v/v) of antibiotic solution (comprised of Fung., L-glutamine and penicillin–streptomycin,)(Sigma-Aldrich).

For initial SEM evaluation, culture medium was removed from the wells after three days culture, and the samples were rinsed in pre-warmed PBS at 37 °C. The cells were then fixed in 1.5% (w/v) glutaraldehyde in 0.1 M sodium cacodylate for 1 h at 4 °C, and rinsed twice, again in 0.1 M sodium cacodylate. The samples were then postfixed in osmium tetroxide for 1 h, rinsed three times in distilled water, stained with 0.5% aqueous uranyl acetate for 1 h in the dark, washed twice in distilled water, and dehydrated in an ethanol series of 30%, 50%, 70%, 90% and 100% ethanol, with the final dehydration step in hexamethyldisilazane.

For immunofluorescence, after 21 days culture, cells were fixed in 4% formaldehyde/PBS, with 1% sucrose at 37 °C for 15 min. When fixed, the samples were washed with PBS, and a permeabilising buffer

(10.3 g sucrose, 0.292 g NaCl, 0.06 g MgCl$_2$, 0.476 g Hepes buffer, 0.5 ml Triton X, in 100 ml water, pH 7.2) was added at 4 °C for 5 min. The samples were then incubated at 37 °C for 5 min in 1% BSA/PBS, followed by the addition of an anti-osteocalcin or anti-osteopontin primary antibody (1:50 in 1% BSA/PBS, OC4-30 from Autogen Bioclear or sc-21742 from Insight Biotech) for 1 h (37 °C). Simultaneously, rhodamine conjugated phalloidin was added for the duration of this incubation (1:100 in 1% BSA/PBS, Molecular Probes, Oregon, USA). The samples were next washed in 0.5% Tween 20/PBS (5 min × 3). A secondary, biotin conjugated antibody, (1:50 in 1% BSA/PBS, monoclonal horse anti-mouse (IgG), Vector Laboratories, Peterborough, UK) was added for 1 h (37 °C) followed by washing. A FITC conjugated streptavidin third layer was added (1:50 in 1% BSA/PBS, Vector Laboratories, Peterborough, UK) at 4 °C for 30 min, and given a final wash. Samples were then viewed by fluorescence microscopy (Zeiss Axiovert 200 M).
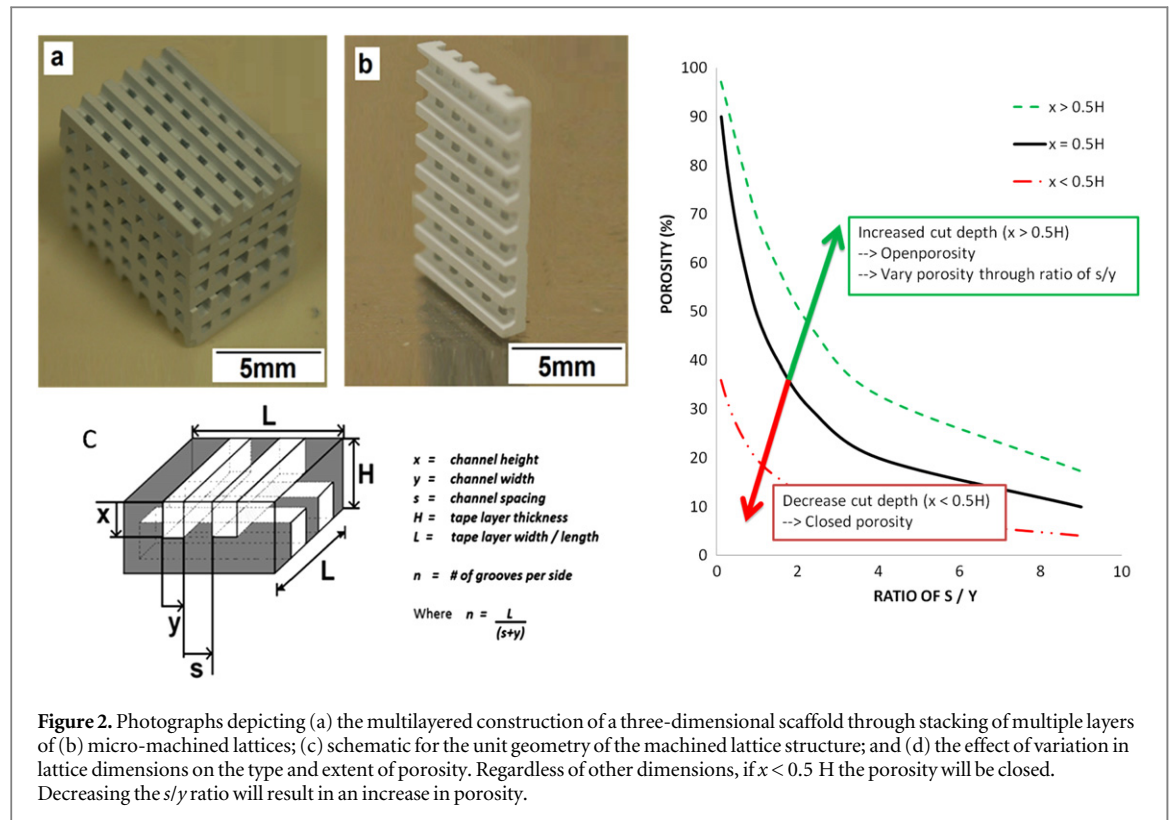
2.7. *In vivo* testing

2.7.1. Animals and surgery

All animal procedures were approved by the Department of Health, Hong Kong SAR. Six female skeletally matured New Zealand white rabbits (average body weight 3.0–3.5 kg) were used. A bilateral 10 mm segmental defect was created in the left and right radial diaphysis. Briefly, the rabbits were anesthetized at a dose of 0.6 ml kg^{-1} by PBS solution containing 5% (w/v) ketamine and 1% (w/v) xylazine through intramuscular injection. Following a 20 mm incision over the middle third of the radius and dissection of the overlying tissues to expose the radial diaphysis, a 10 mm segmental defect was created with an oscillating saw under copious irrigation with normal saline. Rabbits with a 10 mm radial defect were implanted with one of the following three scaffolds: (a) non-patterned control, $n = 4$; (b) 50 μm groove patterned, $n = 4$; (c) 40 μm pits patterned composite substrate, $n = 4$. Immediately after implantation, the soft tissues and the skin were closed with a continuous 3-0 Vicryl suture. After surgery, the rabbits were received an intramuscular injection with 2.5 kU penicillin for three days. Two months after the implantation, the rabbits were killed by over dose of pentobarbital. The whole radius including the implanted biomaterials were collected and fixed in 10% (v/v) phosphate-buffered formalin pH 7.20 for two days and subject to further examinations.

2.7.2. Micro-CT analysis

Micro-CT scanning was conducted using viva CT 40 (Scanco Medical, Switzerland) with a voltage of 70 k eV and a current of 114 μA, to determine the microstructure of the radial defect region. The scanning region covered the whole grafts in radius, with the

Figure 2. Photographs depicting (a) the multilayered construction of a three-dimensional scaffold through stacking of multiple layers of (b) micro-machined lattices; (c) schematic for the unit geometry of the machined lattice structure; and (d) the effect of variation in lattice dimensions on the type and extent of porosity. Regardless of other dimensions, if $x < 0.5$ H the porosity will be closed. Decreasing the s/y ratio will result in an increase in porosity.

length of 1.043 cm in each scanning (voxel size = 38 μm). The contoured regions of interest (ROI) were selected from 2D CT images covering the whole bone (with both grafts and original bone). 3D reconstructions of mineralized tissues were performed using a low-pass Gaussian filer (sigma = 1.2, support = 2) with the same threshold (attenuation = 190). The following morphometric parameters were evaluated by the built-in software: total volume (TV), bone volume (BV), relative BV (BV/TV) and bone mineral density (BMD). In this study, the ROI was defined as the entire bone defect region (with the biomaterials), and we have measured BV/TV and BMD (as parameters for estimating bone quality as well as quantity) of the selected regions and compared them among the different groups.

2.7.3. Histological analysis

After micro-CT analysis, the specimens were decalcified in 9% (v/v) formic acid for three weeks, following dehydration through a series of increasing concentrations of ethanol and cleared in xylene. Specimens were then embedded in paraffin. 5 μm sections were cut with a microtome (Leica RM2155, Germany) strictly paralleled to the axis of the radius. Each section was then stained with haematoxylin and eosin and analyzed under microscopy.

2.7.4. Statistics

All results were expressed as the mean ± standard deviation. The *p* value of 0.05 was used in the

calculation to determine whether there were any significant differences between any two groups. The One-Way ANOVA Tukey's test using SPSS software v16.0 (SPSS, Chicago, IL, USA) was used to assess the statistical significance of difference.

3. Results and discussion

3.1. 3D lattice scaffold fabrication and evaluation

With the use of subtractive microfabrication via CNC machining a grid of specific dimensions can be machined into either side of the composite substrates. By stacking these layers together we are able to construct a 3D, porous lattice scaffold for bone tissue engineering (figures 2(a) and (b)).

3.1.1. Lattice geometry and porosity

The schematic shown in figure 2(c) represents the geometry of a single lattice layer and serves as a model for analysis of the macroporosity of the 3D scaffold. Through simple algebra, the following (equation (1)) relationship, based on lattice fabrication on a 5×5 cm^2 area, was derived to express the result of variation in lattice geometry and the corresponding porosity. A wide range of porosities can be achieved via adjustment of channel width, height and/or spacing of the machined channels.

$$\text{Porosity \%} = \frac{200\,nxy}{LH}$$
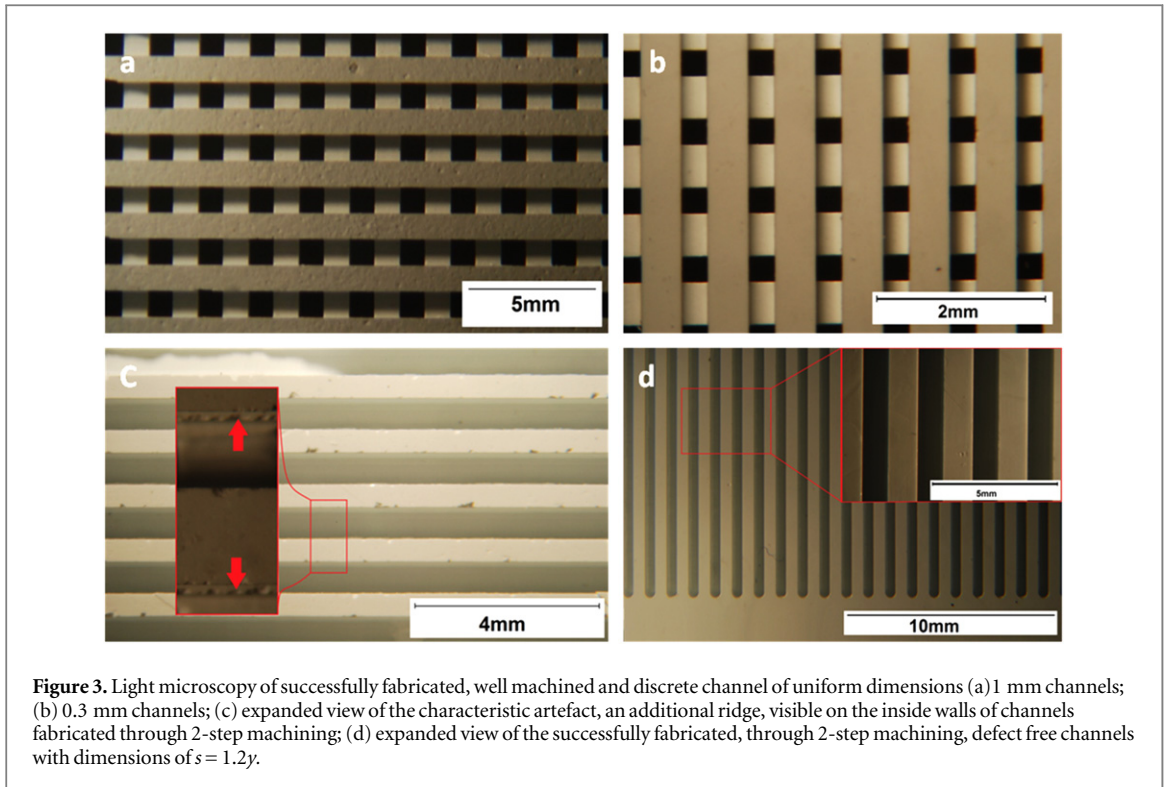$$(x \leqslant H/2).\qquad (1)$$

Figure 3. Light microscopy of successfully fabricated, well machined and discrete channel of uniform dimensions (a) 1 mm channels; (b) 0.3 mm channels; (c) expanded view of the characteristic artefact, an additional ridge, visible on the inside walls of channels fabricated through 2-step machining; (d) expanded view of the successfully fabricated, through 2-step machining, defect free channels with dimensions of $s = 1.2y$.

Note that in order to ensure an open and continuous porosity, as opposed to closed cell porosity, micromachined channels on either face must intersect (figure 2(d)) i.e. $x > H/2$, thus creating an interconnected and open porosity. For $x > H/2$, the volume occupied by the intersection of channels from either side must then also be accounted for, as demonstrated by equation (2).

$$\text{Total volume}_{\text{(channel intersection)}} = 2n^2 y^2 \times \left(x - \frac{H}{2} \right). \quad (2)$$

This allows us to further derive the following relationship (equation (3)) between lattice geometry and the resultant porosity. Implementation of this equation enables calculation of the porosity, demonstrating how variation in each parameter affects the porosity of the lattice. As further illustrated by figure 2 (d), the theoretical porosity is highly dependent upon the ratio of channel width to channel spacing (*s/y*) as well as upon the ratio of channel depth (*x*) to substrate thickness (*H*):

$$\text{Porosity\%} = \frac{200\, ny\, (Lx - ny\,(x - H/2))}{L^2 H}$$
$$(x > H/2) \quad (3)$$

where *n* is a natural number (positive integer) and *L*, *H*, *s*, *x*, *y* are real numbers.
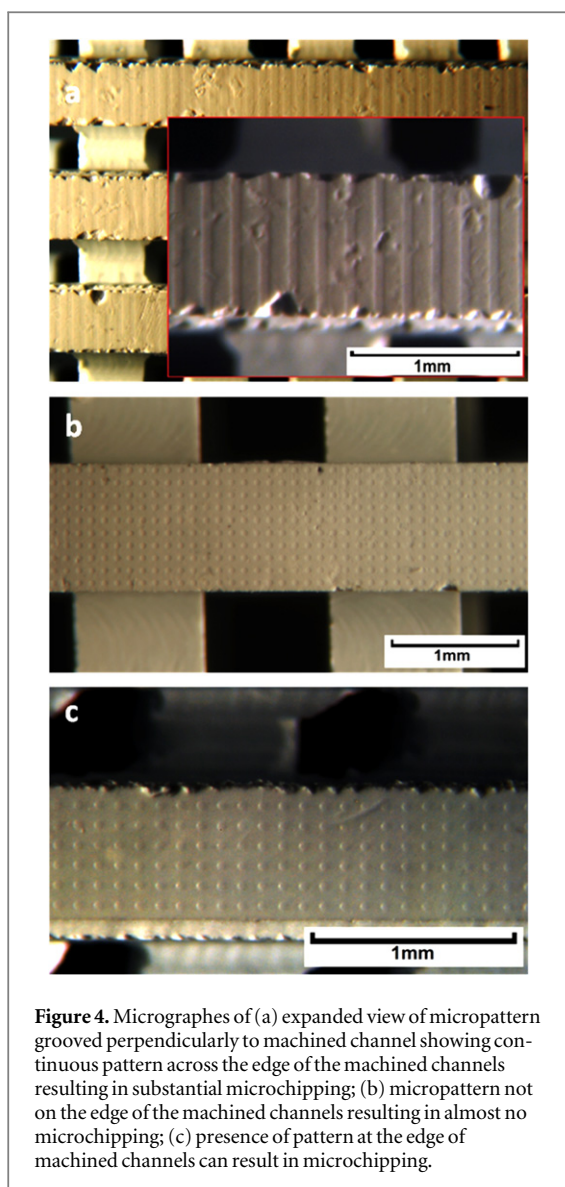
3.1.2. Machinability of composite tape

When considering microfabrication, the first objective was to ensure that the composite is machinable. Confirmation of the green ceramic composite's machinability was attained through visual inspection and micrographs of various channel dimensions. As apparent in figures 3(a) and (b), CNC machining of the composite tape successfully produced discrete channels of uniform dimensions, with few visible defects on the machined surfaces and edges. The swarf produced by machining was found to be discontinuous and powdered in nature, providing confirmation of good quality machining [27]. Using a series of drill attachments, various lattice geometries of 0.2 mm were fabricated; including lattices machined using the smallest available drill attachment of 0.2 mm in diameter. The successful fabrication of multiple lattices confirmed the versatility of the fabrication method as well as validating the possibility of fabricating scaffolds of various geometries for different applications.

In an effort to reduce the minimum channel spacing, a 2-step machining process was encoded to eliminate issues of excessive tape deformation and drill-bit breakage. Although use of the 2-step machining regime effectively reduced the incidence of channel collapse (figure 3(c)), an artefact of the machining process, visible only on the inside surface of the machined channels, was observed (expanded view, figure 3(c)). The appearance of this additional ridge is due to a small shift in position attributed to instrumental error upon reversal of the cutting direction.

An additional benefit of the 2-step machining can be seen in the effective reduction of the minimum machinable spacing to approximately $s \approx 1.2y$, as shown by the successful machining of defect-free channels with the following geometry; $y = 0.5$ mm, $s = 0.6$ mm (figure 3(d)).

Figure 4. Micrographes of (a) expanded view of micropattern grooved perpendicularly to machined channel showing continuous pattern across the edge of the machined channels resulting in substantial microchipping; (b) micropattern not on the edge of the machined channels resulting in almost no microchipping; (c) presence of pattern at the edge of machined channels can result in microchipping.

Figure 5. Representative SEM images of adherent cells on the non-patterned surface (a) showing polarized cell morphology; micro-grooved surface (b); and micro-pitted surface (c), showing hOPCs exhibiting more polygonal morphologies on micropatterned surfaces.

3.1.3. Machining quality after micropattern embossing
The emergence of microchips along the channel edges of the micromachined composite was observed along several machined edges, most noticeably on samples embossed with the 50 μm groove pattern, aligned perpendicular to the direction of machining (figure 4(a)). In the case of this particular micropattern, the embossed grooves are continuous across the width of the composite surface between machined channels. Additionally, the micropatterned grooves are of a relatively closer order of magnitude ($\sim 10^{-5}$ m) to the size of the ceramic particles ($\sim 10^{-6}$ m) compared to the size of the machined channels ($\sim 10^{-2}$ m), thereby increasing the potential for the occurrence of fracturing due to the shear forces experienced at the machined edges. In contrast, samples embossed with the 40 μm pit pattern exhibited very little fracturing of the machined edge, as illustrated by figure 4(b). The much finer machined edge in this case can be attributed to the fact that the micropattern is rarely present at the edge of the machined channel. However,
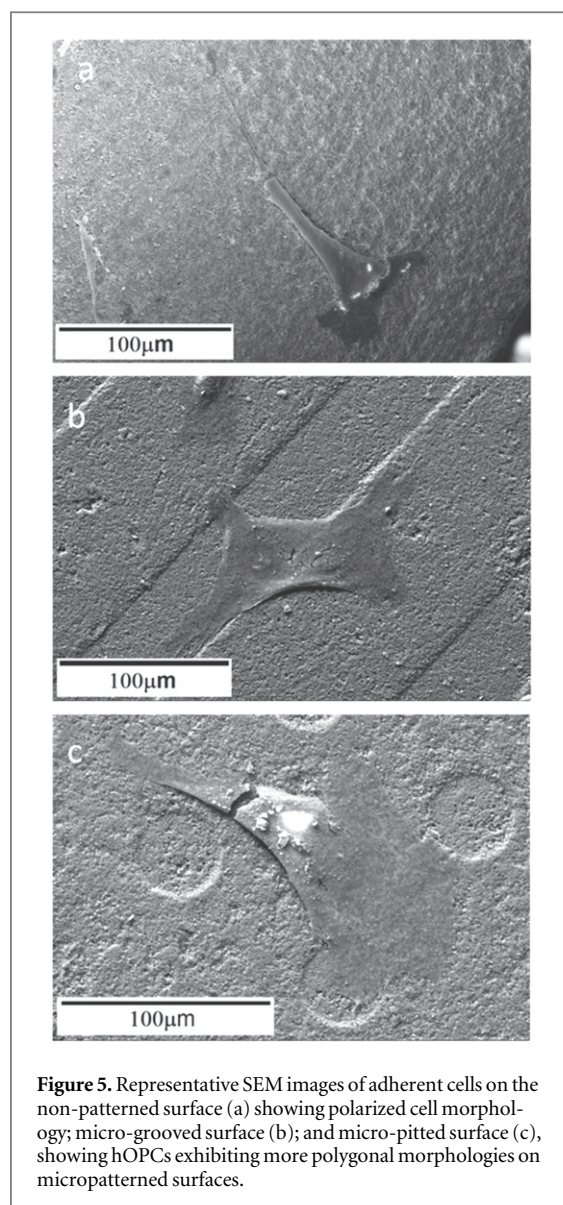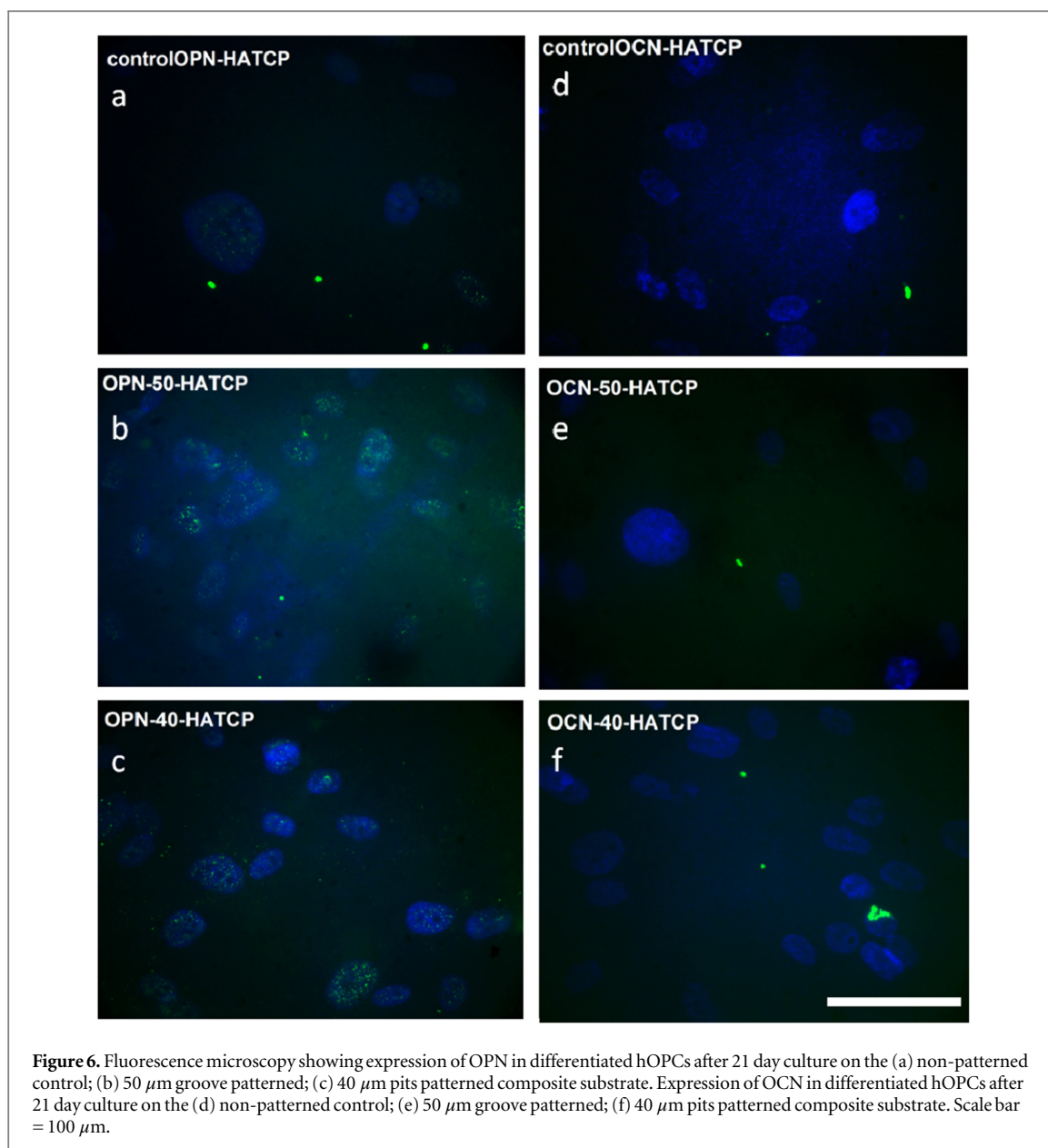
in the event of the micropattern being present at the machined edge, microchipping can once again be observed (figure 4(c)).

3.2. Cellular evaluation of microtopographies on composite substrates
Cells with typical polarized fibroblast morphology were observed on the planar control substrate (figure 5(a)). However, on the grooves (figure 5(b)) and pits (figure 5(c)), the cells were seen to be more polygonal with wide lamellae. This change in morphology is potentially indicative of differentiated cells of osteoblastic lineage [14, 28, 29].

As illustrated in figure 6, compared to the non-patterned control (a) an increased level of expression of OPN and OCN was observed on substrates with the 50 μm (b) and 40 μm (c) topographies after 21 days on culture. It is noteworthy that enhanced OCN expression was only noted on the 40 μm pits (c).

Although the expression of OPN can be used as an indicator of cellular differentiation, its expression is

Figure 6. Fluorescence microscopy showing expression of OPN in differentiated hOPCs after 21 day culture on the (a) non-patterned control; (b) 50 μm groove patterned; (c) 40 μm pits patterned composite substrate. Expression of OCN in differentiated hOPCs after 21 day culture on the (d) non-patterned control; (e) 50 μm groove patterned; (f) 40 μm pits patterned composite substrate. Scale bar = 100 μm.

not limited to osteogenic differentiation and can also associated with various other cell types, such as fibroblasts [30] or myoblasts [31]. As such, a more conclusive indication of the induction of osteogenic differentiation is necessary and can be found in the corresponding degree of OCN expression, on the patterned and non-patterned substrates. The expression of OCN markers is exhibited exclusively by osteoblasts so it provides a more definitive assessment of osteogenic differentiation. In terms of its expression, OCN is expressed post-proliferatively, lagging behind the expression of OPN [32] as so 21 days is quite a short culture time-point to study OCN at. As a result, a comparison between the expression of OPN and the corresponding expression of OCN, for the different topographies, can be used to further differentiate the observed similarly inductive response (based on OPN expression) of the 50 μm and 40 μm topographies, in terms of the progression of osteogenic differentiation. This can be demonstrated by the negligible expression of OCN on all topographies apart from the 40 μm micro-pits. The beginning of OCN expression on the pits indicates that the osteogenic differentiation had progressed further than on any other topography, thereby establishing its comparatively increased inductive potential of osteogenic differentiation.

These data tie in well with previous studies on polymers. While narrow grooves are highly aligning to cells initiating contact guidance and bipolar morphology, very wide grooves, such as the 40 μm pits and 50 μm grooves used here, provide step cues to cells which increase cell spreading and osteogenesis [33, 34]. Micropatterning of 40 μm diameter pits into fibrous hydrogels has shown to increase osteoblast marker expression in osteosarcoma cells [35] and >30 μm micro-pits embossed in polycaprolactone
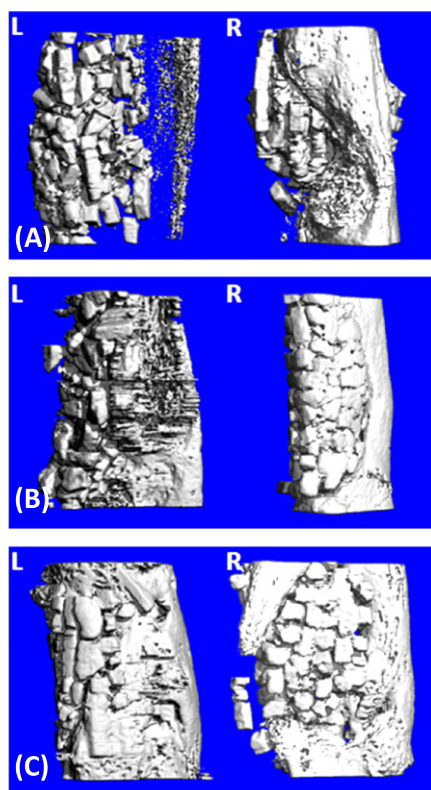
Figure 7. The representative 3D reconstruction images of the micro-CT scanned region. Bone-scaffold integration was better and more new bone was formed in either the 50 μm groove patterned (B) or the 40 μm pits patterned groups (C) after two months' implantation compared with the non-patterned control group (A). (L, left side radius; R, right side radius).

have been shown to be osteogenic to primary osteo-progenitor populations [36, 37]. Hence, we can have confidence in our data to move to an *in vivo* study.

3.3. *In vivo* results

The 3D reconstruction images of the scanned region were shown in figure 7, with the quantitative data showed in figure 8. Compared with the non-patterned control group, bone-scaffold integration was better and more new bone was formed in either the 50 μm groove patterned or the 40 μm pits patterned groups after two months' implantation. The data also indicated that BV, BMD, and BV/TV in the 40 μm pits patterned composite substrate and the 50 μm groove patterned groups were all significantly higher than those in the control group ($p < 0.05$), while no significant difference was found between the two patterned groups.

For the histology examinations, both scaffolds remnants and newly formed bone were observed in the gap at the radius in all the groups. Consistent with the micro-CT data, diffuse bone formation was observed within the scaffold as well as in the periphery of the scaffolds in all samples. More mature ossified tissues and callus formation was seen in the scaffolds with the 50 μm grooves patterned and the 40 μm pits patterned groups, in contract to the non-patterned control group (figure 9).

The *in vivo* results clearly demonstrated the benefit of surface microtopography to new bone formation, which is desirable for bone tissue engineering
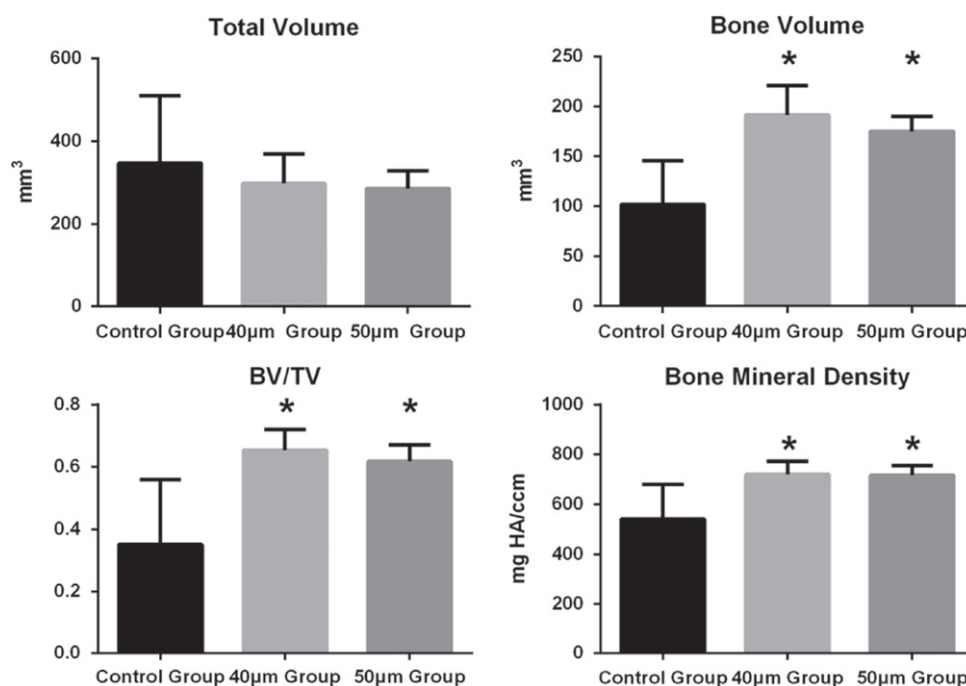

Figure 8. Quantitative data of micro-CT analysis for scaffold region in rabbit radius. *$p < 0.05$, the 50 μm groove patterned or the 40 μm pits patterned groups versus non-patterned control group.
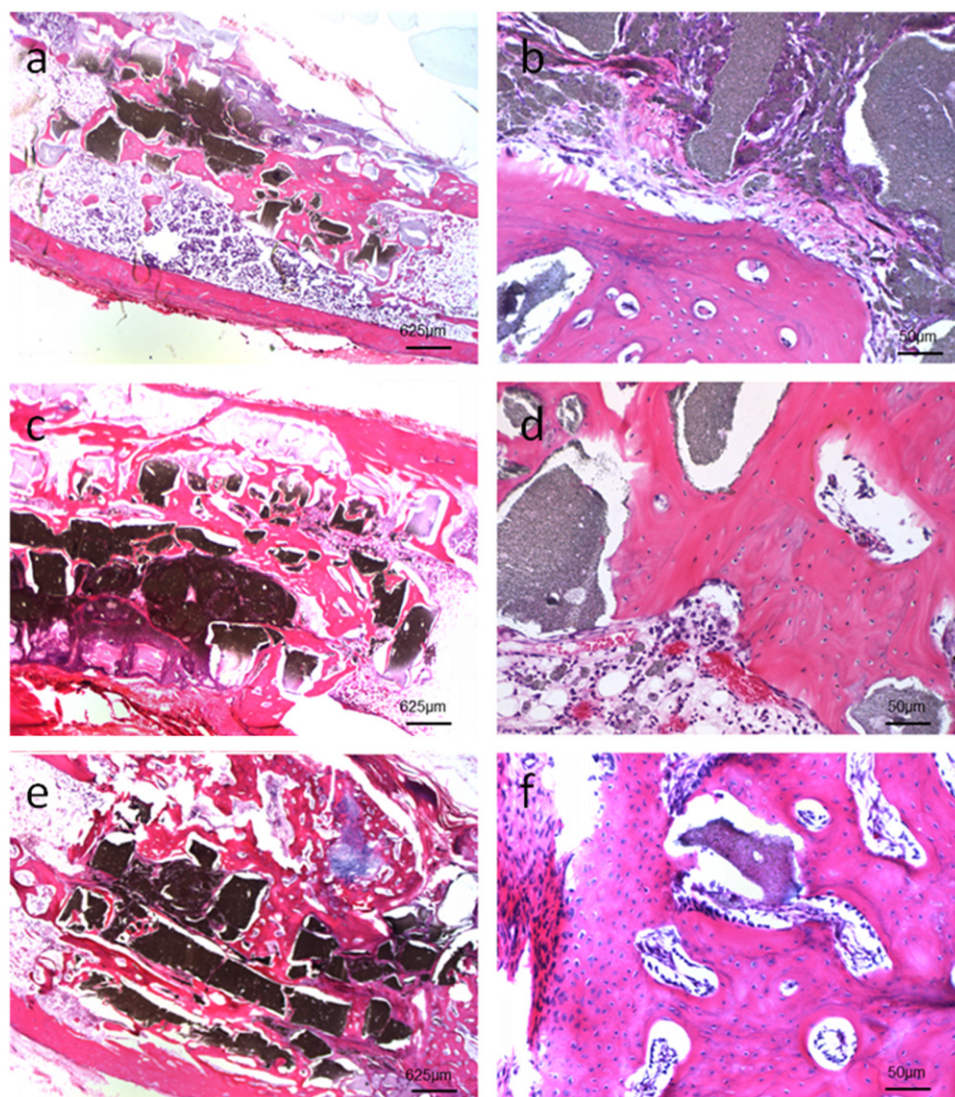
Figure 9. Microscopic images of the longitudinal sections of the radius with scaffolds after two months' implantation. (a) and (b): the non-patterned control samples; (c) and (d): the 50 μm groove patterned samples; (e) and (f): the 40 μm pits patterned samples. Diffused bone formation was observed within the scaffolds as well as along the surfaces of the scaffolds in all samples. More mature ossified tissues and callus formation is observed in the scaffolds with the 50 μm groove patterned and the 40 μm pits patterned groups than that of the non-patterned control group. (a)–(f), *H* and *E* staining, (a), (c), (e) × 100 magnification; (b), (d), (f) × 400 magnification, with bar scale.

applications. Such micropatternes can not only be achieved in 2D implants as we reported previously [13, 14], but also in 3D scaffolds if a suitable fabrication process could be established.

4. Conclusions

We have demonstrated a novel fabrication process for 3D bone tissue engineering scaffolds with defined surface topographies. By optimising the composition of composites, machining parameters, and embossing conditions, it is possible to produce 3D lattices of pore size of >200 μm with variable porosities. CaP/gelatin composite scaffolds with surface micropatterns of 40 μm pits and 50 μm grooves have exhibited enhanced osteoinductivity and osteogenesis in both *in vitro* and *in vivo* studies compared to those without

surface micropatterns. The results clearly indicate the potential of creating 3D scaffolds capable of inducing specific cellular responses by physical cues via surface topography. The fabrication process offers distinct advantages over other scaffold manufacturing techniques such as 3D printing and direct foaming.

Acknowledgments

Hong Kong, to Li Gang. We also thank Mr Andrew Wilkinson for help with cell culture experiments.

References

[1] Jones J R 2009 New trends in bioactive scaffolds: the importance of nanostructure *J. Eur. Ceram. Soc.* **29** 1275–81

[2] Gentile P, Chiono V, Carmagnola I and Hatton P V 2014 An overview of poly(lactic-co-glycolic) acid (PLGA)-based biomaterials for bone tissue engineering *Int. J. Mol. Sci.* **15** 3640–59

[3] Gombotz W R and Pettit D K 1995 Biodegradable polymers for protein and peptide drug delivery *Bioconjug. Chem.* **6** 332–51

[4] Rohanizadeh R, Swain M and Mason R 2008 Gelatin sponges (Gelfoam ®) as a scaffold for osteoblasts *J. Mater. Sci., Mater. Med.* **19** 1173–82

[5] Ulubayram K, Aksu E, Gurhan S I, Serbetci K and Hasirci N 2002 Cytotoxicity evaluation of gelatin sponges prepared with different cross-linking agents *J. Biomater. Sci. Polym. Ed.* **13** 1203–19

[6] Bigi A, Cojazzi G, Panzavolta S, Rubini K and Roveri N 2001 Mechanical and thermal properties of gelatin films at different degrees of glutaraldehyde crosslinking *Biomaterials* **22** 763–8

[7] Barradas A M C, Yuan H P, van Blitterswijk C A and Habibovic P 2011 Osteoinductive biomaterials: current knowledge of properties, experimental models and biological mechanisms *Eur. Cells Mater.* **21** 407–29

[8] Kanczler J M and Oreffo R O 2008 Osteogenesis and angiogenesis: the potential for engineering bone *Eur. Cells Mater.* **15** 100–14

[9] Swart K M, Keller J C, Wightman J P, Draughn R A, Stanford C M and Michaels C M 1992 Short-term plasma-cleaning treatments enhance *in vitro* osteoblast attachment to titanium *J. Oral. Implantol.* **18** 130–7

[10] Bowers K T, Keller J C, Randolph B A, Wick D G and Michaels C M 1992 Optimization of surface micromorphology for enhanced osteoblast responses *in vitro Int. J. Oral. Maxillofac. Surg.* **7** 302–10

[11] Boyan B D, Bonewald L F, Paschalis E P, Lohmann C H, Rosser J, Cochran D L, Dean D D, Schwartz Z and Boskey A L 2002 Osteoblast-mediated mineral deposition in culture is dependent on surface microtopography *Calcif. Tissue Int.* **71** 519–29

[12] McNamara L E, Burchmore R, Riehle M O, Herzyk P, Biggs M J P, Wilkinson C D W, Curtis A S G and Dalby M J 2012 The role of microtopography in cellular mechanotransduction *Biomaterials* **33** 2835–47

[13] Wilkinson A, Hewitt R N, McNamara L E, McCloy D, Meek R M D and Dalby M J 2011 Biomimetic microtopography to enhance osteogenesis *in vitro Acta Biomater.* **7** 2919–25

[14] Nadeem D, Sjostrom T, Wilkinson A, Smith C A, Oreffo R O C, Dalby M J and Su B 2013 Embossing of micropatterned ceramics and their cellular response *J. Biomed. Mater. Res.* **101A** 3247–55

[15] Studart A R, Gonzenbach U T, Tervoort E and Gauckler L J 2006 Processing routes to macroporous ceramics: a review *J. Am. Ceram. Soc.* **89** 1771–89

[16] Bose S, Roy M and Bandyopadhyay A 2012 Recent advances in bone tissue engineering scaffolds *Trends Biotechnol.* **30** 547–54

[17] Hutmacher D W, Sittinger M and Risbud M V 2004 Scaffold-based tissue engineering: rationale for computer-aided design and solid free-form fabrication systems *Trends Biotechnol.* **22** 354–62

[18] Mata A, Kim E J, Boehm C A, Fleischman A J, Muschler G F and Roy S 2009 A three-dimensional scaffold with precise micro-architecture and surface micro-textures *Biomaterials* **30** 4610–7

[19] Cha H D, Hong J M, Kang T Y, Jung J W, Ha D H and Cho D W 2012 Effects of micro-patterns in three-dimensional scaffolds for tissue engineering applications *J. Micromech. Microeng.* **22** 125002

[20] Lei Y, Peng H X, Yang L and Su B 2008 Fabrication of three-dimensional inter-connective porous ceramics via ceramic green machining and bonding *J. Eur. Ceram. Soc.* **28** 531–7

[21] Teixeira S, Oliveira S, Ferraz M P and Monteiro F J 2008 Three dimensional macroporous calcium phosphate scaffolds for bone tissue engineering *Key Eng. Mater.* **361-363** 947–50

[22] Sung H W, Huang R N, Huang L L and Tsai C C 1999 *In vitro* evaluation of cytotoxicity of a naturally occurring cross-linking reagent for biological tissue fixation *J. Biomater. Sci. Polym. Ed.* **10** 63–78

[23] Harini G S, Gary A M, Norman A L, Yves J C, Jennifer R M and David I S 2008 Genipin-induced changes in collagen gels: correlation of mechanical properties to fluorescence *J. Biomed. Mater. Res.* A **87A** 308–20

[24] Huang-Chien L, Wen-Hisung C, Hsiang-Fa L, Meng-Horng L and Hsing-Wen S 2004 Crosslinking structures of gelatin hydrogels crosslinked with genipin or a water-soluble carbodiimide *J. Appl. Polym. Sci.* **91** 4017–26

[25] Ozeki M and Tabata Y 2005 *In vivo* degradability of hydrogels prepared from different gelatins by various cross-linking methods *J. Biomater. Sci. Polym. Ed.* **16** 549–61

[26] Nadeem D, Kiamehr M, Yang X and Su B 2013 Fabrication and *in vitro* evaluation of a sponge-like bioactive-glass/gelatin composite scaffold for bone tissue engineering *J. Mater. Sci. Eng.* **C33** 2669–78

[27] Dhara S and Su B 2005 Green machining to net shape alumina ceramics prepared using different processing routes *Int. J. Appl. Ceram. Technol.* **2** 262–70

[28] Dalby M J, Riehle M O, Yarwood S J and Wilkinson C D W 2003 Curtis ASG. nucleus alignment and cell signaling in fibroblasts: response to a micro-grooved topography *Exp. Cell Res.* **284** 272–80

[29] Dalby M J, Di Silvio L, Gurav N, Annaz B, Kayser M V and Bonfield W 2002 Optimizing HAPEX topography influences osteoblast response *Tissue Eng.* **8** 453–67

[30] Ashizawa N, Graf K, Do Y S, Nunohiro T, Giachelli C M, Meehan W P, Tuan T L and Hsueh W A 1996 Osteopontin is produced by rat cardiac fibroblasts and mediates a (II)-induced DNA synthesis and collagen gel contraction *J. Clin. Invest.* **98** 2218–27

[31] Uaesoontrachoon K, Yoo H J, Tudor E M, Pike R N, Mackie E J and Pagel C N 2008 Osteopontin and skeletal muscle myoblasts: association with muscle regeneration and regulation of myoblast function *in vitro Int. J. Biochem. Cell Biol.* **40** 2303–14

[32] Lian J B and Stein G S 1995 Development of the osteoblast phenotype: molecular mechanisms mediating osteoblast growth and differentiation *Iowa Orthop. J.* **15** 118–40

[33] Biggs M J, Richards R G, Gadegaard N, Wilkinson C D, Oreffo R O and Dalby M J 2009 The use of nanoscale topography to modulate the dynamics of adhesion formation in primary osteoblasts and ERK/MAPK signalling in STRO-1+ enriched skeletal stem cells *Biomaterials* **30** 5094–103

[34] Biggs M J, Richards R G, McFarlane S, Wilkinson C D, Oreffo R O and Dalby M J 2008 Adhesion formation of primary human osteoblasts and the functional response of mesenchymal stem cells to 330 nm deep microgrooves *J. R. Soc. Interface* **5** 1231–42

[35] Mata A, Hsu L, Capito R, Aparicio C, Hanrikson K and Stupp S I 2009 Micropatterning of bioactive self-assembling gels *Soft Matter* **5** 1228–36

[36] Wilkinson A, Hewitt R N, McNamara L E, McCloy D, Dominic Meek R M and Dalby M J 2011 Biomimetic microtopography to enhance osteogenesis *in vitro Acta Biomater.* **7** 2919–25

[37] Dalby M J, McCloy D, Robertson M, Wilkinson C D and Oreffo R O 2006 Osteoprogenitor response to defined topographies with nanoscale depths *Biomaterials* **27** 1306–15